Available online at www.sciencedirect.com
ScienceDirect
Journal of Non-Crystalline Solids 353 (2007) 4806–4812
JOURNAL OF NON-CRYSTALLINE SOLIDS
www.elsevier.com/locate/jnoncrysol

Crystal structure stability and catalytic activity of magnetoplumbite (MP) catalyst doped with Mn and Mg

Fei Teng [a,*], Yi Man [a], Shuhui Liang [a], G. Buergen [a], Yongfa Zhu [a,*], Wei Han [b], Ping Xu [b], Guoxing Xiong [b], Zhijian Tian [b]

[a] Department of Chemistry, Tsinghua University, Beijing 100084, China
[b] State Key Laboratory of Catalysis, Dalian Institute of Chemical Physics, Chinese Academy of Sciences, Dalian 116023, China

Received 5 September 2006
Available online 14 August 2007

Abstract

$LaMg_xMn_{1-x}Al_{11}O_{19}$ catalysts with Magnetoplumbite (MP) structure were prepared by the reverse microemulsion method, where x values were varied in the range of 0–1. The effects of Mn and Mg introductions on crystalline phase compositions, texture and activities of the catalysts were investigated. The catalysts were characterized by XRD, N_2 adsorption, TEM, H_2-TPR, TG-DTA, etc. The results showed that $LaMg_{0.5}Mn_{0.5}Al_{11}O_{19}$ catalyst had high surface area (40.1 $m^2\ g^{-1}$/1200 °C 5 h); $LaMg_{0.5}Mn_{0.5}Al_{11}O_{19}$ catalyst exhibited the high activity for CH_4 combustion ($T_{10} = 470$ °C, $T_{90} = 690$ °C). It was believed that a synergetic effect of Mg and Mn is beneficial to enhance the stability and catalytic activity of the crystals.

PACS: 68.60.Dv; 64.70.Kb; 05.70.Fh; 61.10.Nz; 61.50.Ks

Keywords: Magnetoplumbite (MP) crystal; Reverse microemulsion; Structure stability; Synergetic effect; CH_4 combustion

1. Introduction

Catalytic combustion of CH_4 at high-temperature is an environmental-benign combustion technology. Compared with flame combustion, CH_4 can burn more efficiently in wider air-to-fuel ratios and NO_x emissions can be reduced greatly [1]. The key of this technology is to design a highly efficient catalyst. Over the decades, hexaaluminates catalysts have been explored extensively [2–11]. In view of synthesis strategy, researchers tried to suppress formation of the impurities crystals (e.g. $LaAlO_3$ or $BaAl_2O_4$, α-Al_2O_3) by enhancing homogeneity of precursor. In particular, $BaAl_{12}O_{19}$ and $CeO_2/BaAl_{12}O_{19}$ catalysts were synthesized by a reverse microemulsion route, which had so far the highest surface area and activity [12]. Nevertheless, the impurities crystals were often segregated during the crystallization process of hexaaluminates, which greatly reduced the activities and stability of the catalysts [13,14].

In view of MP crystallography, the unsubstituted $LaAl_{11}O_{18}$ possesses highly distorted MP structure. $[LaAl_{12}O_{19}]^+$ defective cells are present, which consist of $[Al_{11}O_{16}]^+$ spinel blocks intercalated by mirror planes of $[LaAlO_3]^0$. To maintain electroneutralty of MP crystal, as a result, $[Al_{11}O_{19}]^{5-}$ defective cells are generated. This is characterized by the wide Al excess with respect to the nominal $LaAl_{11}O_{18}$ formulae [2,15,16]. The presence of excess Al would leads to the formation of $LaAlO_3$, which would reduce surface area of catalyst greatly. Therefore, it is not always effective to refrain the formation of impurities crystal by a synthesis strategy. The design of the catalysts with high thermal stability remains a challenge to researchers. To the best of our knowledge, most of endeavors have been devoted to the development of a new synthesis method, but very fewer reports are available on how to refrain the

* Corresponding authors. Tel./fax: +86 10 62787601.
E-mail addresses: teng-fei@mail.tsinghua.edu.cn (F. Teng), zhuyf@mail.tsinghua.edu.cn (Y. Zhu).

0022-3093/$ - see front matter © 2007 Elsevier B.V. All rights reserved.
doi:10.1016/j.jnoncrysol.2007.06.069

segregation of the impurities crystals from the viewpoint of MP crystal structure [15–17]. The divalent metal ions (Mg and Mn) can suppress the segregation of the impurities crystals and is beneficial to reduce the defectivities of MP crystal effectively [3].

In the work, $LaMg_xMn_{1-x}Al_{11}O_{19}$ ($x = 0, 0.2, 0.5, 0.8, 1$) catalysts were synthesized in the reverse microemulsions, using inexpensive inorganic salts as starting chemicals. The samples were characterized by TEM, TG-DTA, XRD, N_2 adsorption, H_2-TPR, etc. The influences of Mg and Mn on physicochemistry properties of MP catalysts were investigated.

2. Experimental

2.1. Catalyst preparation

In the experiment, all chemicals were of chemical grade and purchased from Liaoyang Chemicals Company, Ltd. They were used without further purification. The used reverse microemulsion system consisted of polyoxyethylene (7) Octanyl phenyl alcohol ether (NP7, molecule weight: 464), *n*-hexanol, cyclohexane and aqueous solution of ammonium carbonate (or stoichiometric nitrates), which were employed as surfactant, cosurfactant, continuous phase and dispersed phase, respectively. The reverse microemulsion synthesis strategy of $LaMg_xMn_{1-x}Al_{11}O_{19}$ catalysts is given in Fig. 1.

In a typical procedure, 1.0 M $(NH_4)_2CO_3$ solution and 0.5 M mixture solution of nitrates were used, and the weight ratios of water/$C_{13}E_6$/*n*-butanol/cyclohexane were kept at 1.5:1.2:3.5:13.5. At room temperature, the precursors were synthesized by rapid mixing the equal volumes of nitrates-containing microemulsion and $(NH_4)_2CO_3$-containing microemulsion under vigorous stirring. The reaction continued for 5 h under stirring, and then, the mixture was aged for 24 h under undisturbed condition at room temperature. After aging, acetone was added to demulsify the system, and the precursor was recovered by centrifugation. The precursor was washed sufficiently with deionized water and ethanol in sequence, and then dried by supercritical ethanol drying. Supercritical drying process was operated at 260 °C and 7.0–8.0 MPa for 2 h. The details of the drying method were described elsewhere [18]. The samples were calcined at 800, 900 1000, 1100, 1200 in a muffle under a flowing air for 5 h, respectively. To investigate effect of introduction of Mg and Mn on $LaMg_xMn_{1-x}Al_{11}O_{19}$ catalysts, x value were varied.

2.2. Characterization

The samples were characterized by X-ray diffraction (XRD) on a Rigaku D/MAX-RB X-ray powder diffractometer, using graphite monochromatized Cu Ka radiation ($\lambda = 0.154$ nm), operating at 40 kV and 50 mA. The patterns were scanned from 5° to 70° (2θ) at a scanning rate of 5° min^{-1}. A nitrogen adsorption isotherm was performed at 77 K and $<10^{-4}$ bar on a Micromeritics ASAP2010 gas adsorption analyzer. Each sample was degassed at 200 °C for 5 h before the measurement. Surface area and pore size distribution were calculated by BET (Brunauer–Emmett–Teller) and BJH (Barrett–Joyner–Halenda) methods, respectively. The morphology of the catalyst was characterized with a JEOL model 200CX transmission electron microscope with the accelerating voltage of 200 kV. The powders were dispersed in ethanol ultrasonically, and then the samples were deposited on a thin amorphous carbon film supported by copper grids. TGA–DTA was carried out with Pyris 1 TGA thermogravimeter and DTA-7 (US Perkin-Elmer Co.), and the temperature rises from room temperature to 900 °C at a rate of 10 °C min^{-1}.

2.3. H_2-TPR (Temperature programming reduction)

To evaluate the level of reducible Mn species in the catalyst, H_2-TPR was conducted on Micromeritics 2900 TPD/TPR. About 0.5 g of catalyst was placed in the analyzing instrument and heated from 30 to 900 °C in a flow of He and H_2 (10% H_2 and 90% He) at a heating rate of 10 °C min^{-1}. Outlet H_2 concentration was monitored using a thermal conductivity detector (TCD), which allowed the evaluation of H_2 consumption.

2.4. Combustion of CH_4 over the catalysts

The reaction of CH_4 combustion was carried out in a conventional flow system under atmospheric pressure. 0.5 ml catalyst (20–40 mesh) was mixed with 0.5 ml quartz powder, and then was loaded in a quartz reactor (i.d. 10 mm), with quartz beads packed at both ends of the catalyst bed. A mixture gas of 1 vol.% CH_4 and 99 vol.% air was fed into the catalyst bed at a gas hourly space velocity

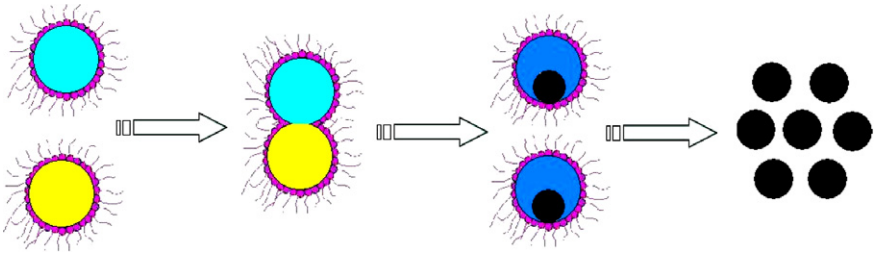

Fig. 1. Diagram of reverse microemulsion synthesis of $LaMg_xMn_{1-x}Al_{11}O_{19}$ catalysts.

(GHSV) of 48 000 h^{-1}. The inlet and outlet gas compositions were analyzed by an on-line gas chromatography with a packed column of carbon molecular sieve and a thermal conductivity detector (TCD). Here, T_{10} and T_{90} are used to express the catalyst activity, in which T_{10} and T_{90} were designated as the temperatures at 10% and 90% conversions of methane, respectively.

3. Results and discussion

3.1. Texture and thermal properties of $LaMg_{0.5}Mn_{0.5}Al_{11}O_{19}$ sample

The texture and thermal properties of $LaMg_{0.5}Mn_{0.5}Al_{11}O_{19}$ catalyst were investigated. Fig. 2 gives adsorption isotherms and pore size distributions of $LaMg_{0.5}Mn_{0.5}Al_{11}O_{19}$ catalyst and its precursor by supercritical drying. It could be found that both of them show type-IV isotherms (H_2 hysteresis loops), indicating the interesting mesopores were formed predominantly. The mostly probable pore size of the precursor is 9.6 nm, and the pore size distribution is narrow (Fig. 2(a)). This may indicate the formed nanoparticles were homogeneous. This

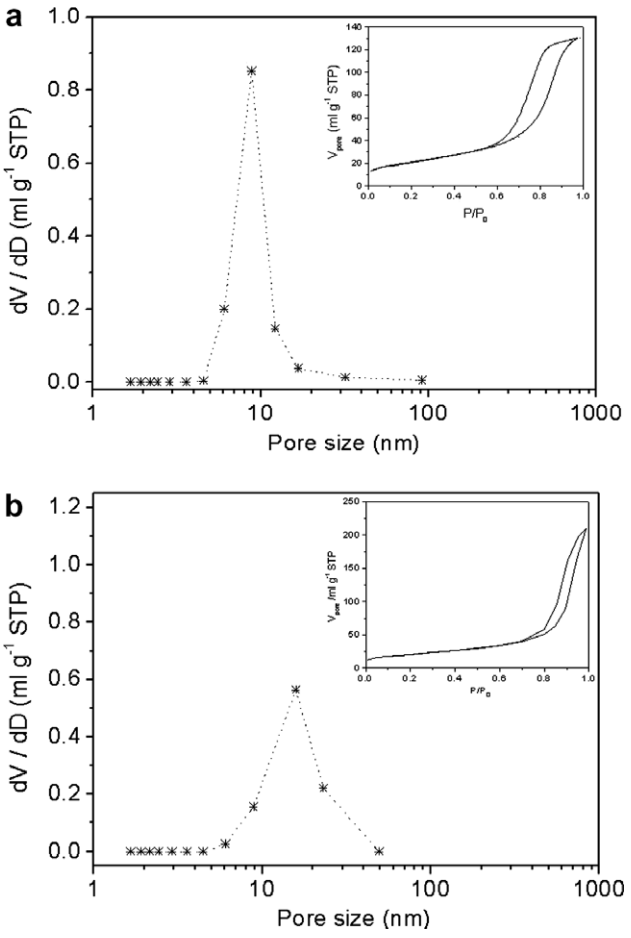

Fig. 2. Adsorption isotherms (inserted parts) and pore size distributions of the samples: (a) precursor by supercritical drying; (b) $LaMg_{0.5}Mn_{0.5}Al_{11}O_{19}$ catalyst calcined at 1200 °C for 5 h.

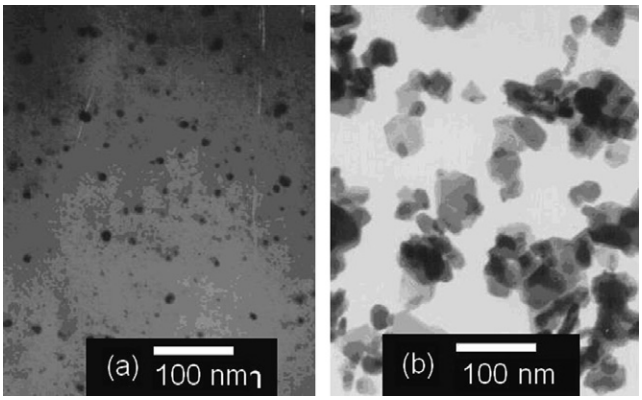

Fig. 3. TEM images of the samples: (a) Dried precursor; (b) $LaMg_{0.5}Mn_{0.5}Al_{11}O_{19}$ catalyst calcined at 1200 °C for 5 h.

is consistent with the results of TEM. Observed from Fig. 3(a), the precursor is composed of the homogeneous particles of 10–20 nm in size. Since the nucleation and growth of the grains were confined in the nanoscale micelles, it is easy to form the homogeneous nanoparticles [12]. The liquid–gas interface would disappear when the solvent is under the supercritical state. Thereby, the capillary stresses of hydrogel caused by surface tension would be avoided when the hydrogel is dried under the supercritical conditions of ethanol. As a result, the agglomeration of the particles was refrained effectively, and then the homogeneous nanoparticles were formed. The homogeneous nanoparticles packed closely to form the pores with a narrow pore size distribution. After calcination at high temperatures, the growth or agglomeration of the particles occurred. As a result, $LaMg_{0.5}Mn_{0.5}Al_{11}O_{19}$ catalyst is composed of the particles of 30–100 nm in size (Fig. 3(b)). The large particles packed to generate the large pores. Fig. 2(b) shows that the mostly probable pore size of the catalyst is 20 nm in size.

TGA and DTA analyses were also carried out to investigate the thermal properties of the sample. TG-DTA results are shown in Fig. 4. TG curve presents two stages of weight loss in the range of room temperature to 600 °C. Below 200 °C, the weight loss of the sample is about 10%, which

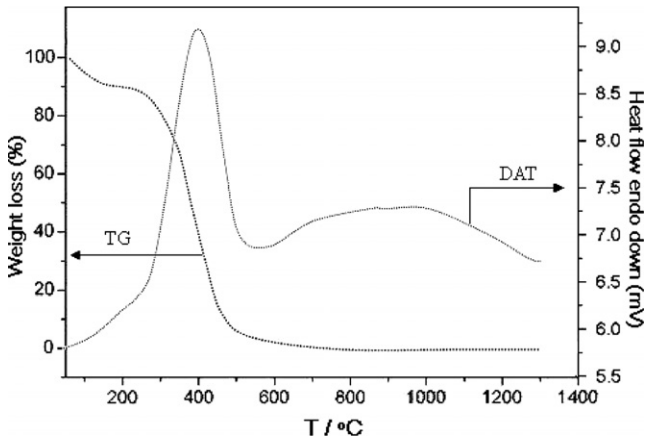

Fig. 4. TGA and DTA curves of $LaMg_{0.5}Mn_{0.5}Al_{11}O_{19}$ precursor sample.

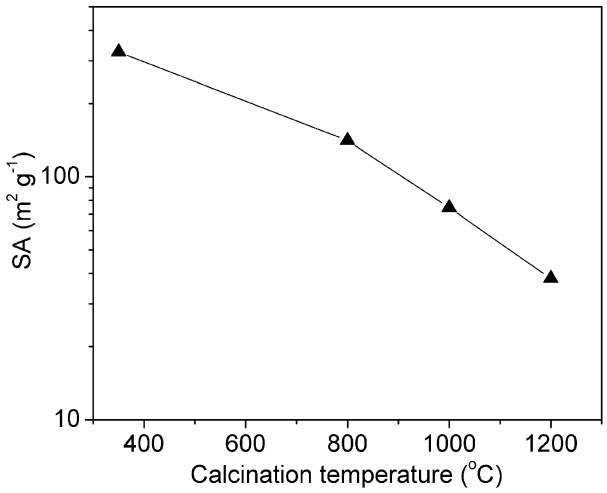

Fig. 5. Surface areas of $LaMg_{0.5}Mn_{0.5}Al_{11}O_{19}$ samples as a function of calcination temperature.

is caused by the dehydration. Above 200 °C, the weight loss of the sample is about 90%. This may be mainly caused by the removal of organic chemicals and hydroxyls, and the decomposition of the carbonates. During the stage, the combustion of the organic chemicals is exothermic; but the hydroxylation and the decomposition of the carbonates are endothermic. Ultimately, an exothermic peak can be observed between 200 and 600 °C in the DTA curve. Above 600 °C, no weight loss and exothermic peak can be observed in the TG curve and DTA curves, respectively. The formation of hexaaluminate phase may be a slow process, or the exothermic effect due to the decrease of surface energy may be small under the experiment conditions [18]; therefore, it is difficult to determine accurately the initial formation temperature of the hexaaluminate phase.

As we know, phase transformation generally resulted in the significant decrease of surface area of the sample. The variations of surface areas of the sample with calcination temperatures were investigated, shown in Fig. 5. The dried sample had surface area of 325 $m^2 g^{-1}$. With increasing of temperature, the surface areas of the sample decreased slightly under protecting of the adsorbed surfactant molecules on surface. At 800 °C, the sample remained high surface area of 150 m g^{-1}. Above 800 °C, the surface area of the sample decreased markedly. This suggests the initial formation of MP crystal. It may be assumed that the sample initially crystallized in the range of from 800 to 900 °C, which could be supported by XRD patterns of the sample in latter (Fig. 6(c)). At 1200 °C, the sample crystallized perfectly, and $LaMg_{0.5}Mn_{0.5}Al_{11}O_{19}$ catalyst had surface area of 40.1 m g^{-1}.

3.2. Influence of Mn and Mg introduction on the structure stability of MP crystal

XRD patterns were performed to investigate crystalline phase compositions of the samples, as shown in Fig. 6. Several interesting features are observed as blow.

Firstly, below 800 °C, all the samples are amorphous, and no diffraction peaks of Mn, Mg and La carbonates (hydroxides or oxides) can be found. This suggests that the constitutes in precursors were mixed homogeneously. Secondly, while $x = 0$, 0.2, 0.5, 0.8, 1, the diffraction peaks of MP crystal appeared at 900, 900, 1000, 1000 and 1000 °C, respectively. It is obvious that at high Mn concentration ($x = 0$, 0.2), the initial formation temperatures of MP crystal are lower than those of the samples at lower Mn concentration. The crystallization of MP crystal appeared to be markedly dependent on the compositions of the samples. Possibly, the low initial formation temperatures can be ascribed as to the high mobility of Mn ion, which was closely related to the small radii of Mn ion (0.64 nm). Moreover, it has been reported that Mn ion speeded up phase transformation of alumina that is involved in β-Al_2O_3-typed hexaaluminates [2]. We could assume that MP crystal could be favored by the same mechanism for β-alumina. Lastly, a significant amount of $LaAlO_3$ impurities crystal are present for $LaMg_xMn_{1-x}Al_{11}O_{19}$ at $x = 0$ and 0.2. With increasing of Mg loading, the intensities of diffraction peaks of $LaAlO_3$ decreased gradually. At $x > 0.5$, the diffraction peaks of $LaAlO_3$ crystal nearly disappeared, since the presence of Mn could also promote the formation of $LaAlO_3$ simultaneously [2].

The texture properties of $LaMg_xMn_{1-x}Al_{11}O_{19}$ catalysts are shown in Table 1. At $x = 0$ and 0.2, the catalysts have surface areas lower than 30 $m^2 g^{-1}$, which may be due to the segregation of $LaAlO_3$. This caused additional sintering of the catalyst. At $x = 0.5$, the catalyst reached the maximum surface area of 40 $m^2 g^{-1}$ due to a synergetic effect of Mn and Mg, in which Mn promoted the formation of MP structure and Mg stabilized the MP structure. At $x = 0.8$ and 1, the surface areas of the catalysts decreased slightly possibly due to high initial crystallization temperatures of MP crystal. However they maintained surface areas higher than 30 $m^2 g^{-1}$. Observed from Fig. 6, the initial formation temperature of MP crystal increased with increasing of Mg loading. Possibly, the high initial formation temperatures can be ascribed as to the low mobility of Mg ion, which was closely related to the large radii of Mg ion (0.72 nm). After the catalysts were calcined at 1200 °C for 10 h, the surface areas of $LaMnAl_{11}O_{19}$ decreased significantly, but those of others did not decreased. This may be related to the catalyst composition.

In order to investigate the oxidation states of Mn in MP structure, H_2-TPR measurements were performed on $LaMg_xMn_{1-x}Al_{11}O_{19}$ catalysts. Two reduction peaks can be identified from Fig. 7. The maximum of the first peak locates at ~450 °C, and the second at ~700 °C. Since the second peak at ~700 °C plays a minor role in CH_4 combustion; therefore, the first reaction is mainly considered in this work. Compared with TPR spectra of pure manganese oxides [19,20], the temperatures of the peaks are close to that of Mn_2O_3 and that of the spinel Mn_3O_4. Furthermore, it has been reported that [21,22]. Mn preferentially enters the structure as Mn(II) in tetrahedral holes and as Mn(III)

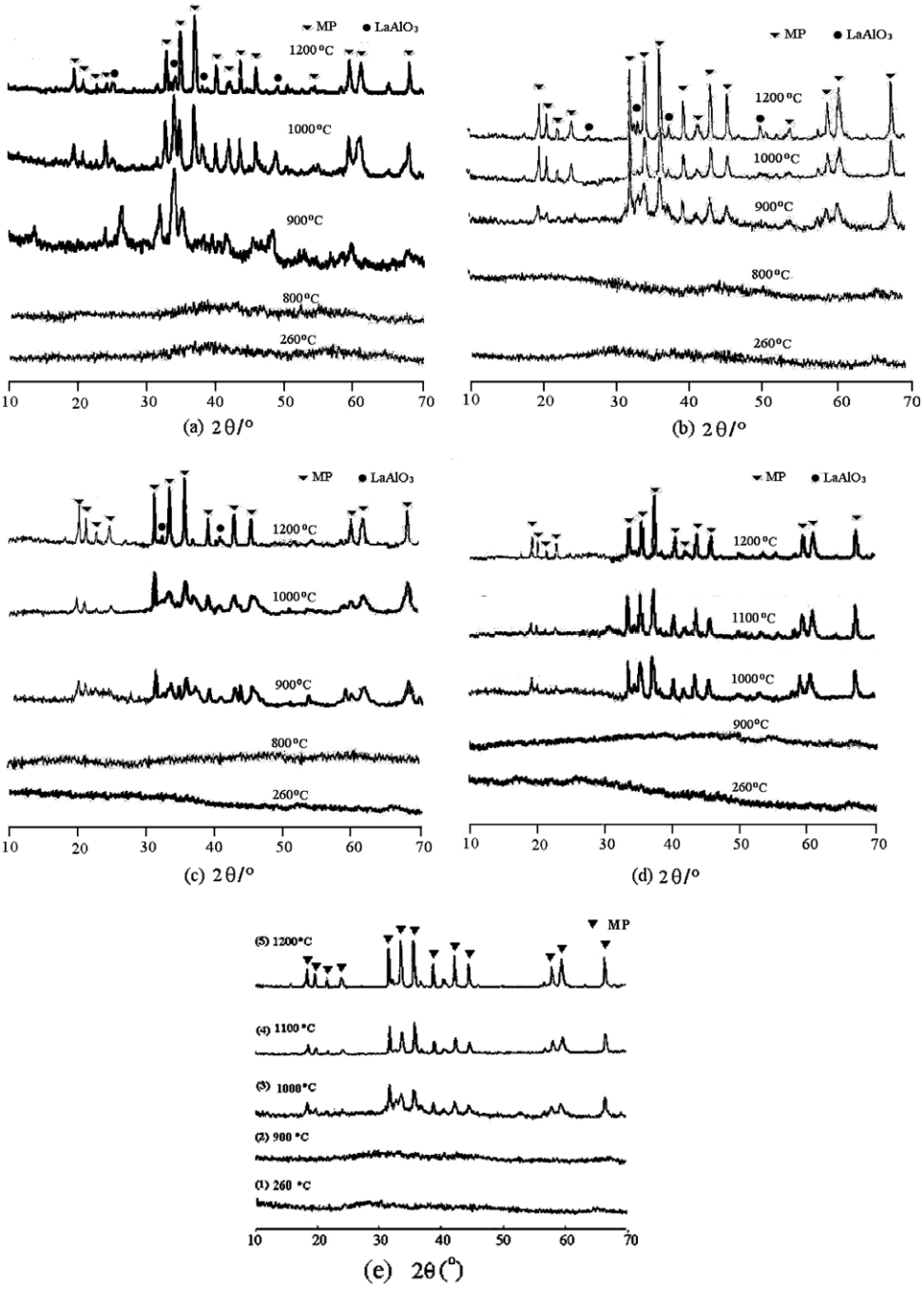

Fig. 6. XRD patterns of $LaMg_xMn_{1-x}Al_{11}O_{19}$ samples: (a) $x = 0$, (b) $x = 0.2$, (c) $x = 0.5$, (d) $x = 0.8$, (e) $x = 1$. Notes: (a, b) indexed to JCPDS 36-1317; (c, d, e) indexed to JCPDS 26-873; $LaAlO_3$, indexed to JCPS 31-22.

Table 1
Texture properties of $LaMg_xMn_{1-x}Al_{11}O_{19}$ catalysts

Catalyst	SA ($m^2\ g^{-1}$)[a]	SA ($m^2\ g^{-1}$)[b]
$x = 0.0$	29.7	24.5
$x = 0.2$	21.5	22.5
$x = 0.5$	40.1	41.3
$x = 0.8$	35.5	34.2
$x = 1.0$	33.3	32.0

[a] Calcined at 1200 °C for 5 h in air.
[b] Calcined at 1200 °C for 10 h in air; SA Surface area calculated by BET method.

in octahedral sites for hexaaluminates (β-Al_2O_3). It could be inferred that the first reduction peak could be ascribed as to the reaction of $Mn^{3+} \rightarrow Mn^{2+}$. More importantly, in consideration of Mn content, $LaMg_{0.5}Mn_{0.5}Al_{11}O_{19}$ catalyst contains 50 mol% Mn in $LaMnAl_{11}O_{19}$, but peak area of the first peak decreased non-proportionally to Mn. This means that more Mn ions with high oxidation state were present in $LaMg_{0.5}Mn_{0.5}Al_{11}O_{19}$ than those of $LaMnAl_{11}O_{19}$ if at the same Mn content [2]. It could be concluded that the introduction of Mg made more Mn to

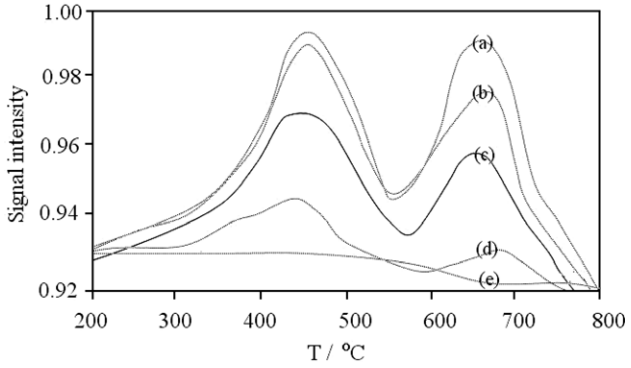

Fig. 7. H_2-TPR profiles on $LaMg_xMn_{1-x}Al_{11}O_{19}$ catalyst: (a) $x = 0$; (b) $x = 0.2$; (c) $x = 0.5$; (d) $x = 0.8$; (e) $x = 1$

take on trivalent state, which is beneficial to enhance the activity of the catalyst. This could be understood in view of MP structure. According to the reports [2,3,15], the parent $LaAl_{11}O_{18}$ have a much distorted MP structure due to its high defectivity. The structure consists of $[Al_{11}O_{16}]^+$ spinel blocks intercalated by mirror planes of composition $[LaAlO_3]^0$. This composition results in an electrically charged cell $[LaAl_{12}O_{19}]^+$, which is required to maintain the electroneutrality. The final structure consists of non-defective $[LaAl_{12}O_{19}]^+$ and defective $[Al_{11}O_{19}]^{5-}$ cells at a molar ratio of 5 to 1, which corresponds to a neutral composition $La_{0.833}Al_{11.833}O_{19}$ (i.e. Al/La = 14.2). This is characterized by a wide Al excess with respect to the nominal $LaAl_{11}O_{18}$ composition. Considering the crystallographic evidence above, it is evident that the substitution of bivalent ions in the spinel blocks for Al^{3+} is an effective alternative to Al excess to maintain electroneutrality of the structure. Substitution of divalent Mn and Mg for trivalent Al could effectively reduce the defectivities of MP structure via a charge compensation mechanism [5], so that the stability of MP structure could be enhanced greatly. According to literatures [21–24], Mg^{2+} enters the structure in tetrahedral sites; and Mn preferentially enters the structure as Mn^{2+} in tetrahedral holes and as Mn^{3+} in octahedral sites for hexaaluminates. In the presence of Mg and Mn, it is not necessary for bivalence Mn to stabilize MP structure. As a result, Mn, as a high oxidation, would prefer to enter the octahedral position. This would be favor for oxidizing reaction of CH_4.

3.3. CH_4 combustion over $LaMg_xMn_{1-x}Al_{11}O_{19}$ catalysts

Fig. 8 gives the light-off curves of CH_4 combustion over $LaMg_xMn_{1-x}Al_{11}O_{19}$ catalysts. At $x \leqslant 0.5$, the ignition temperatures (T_{10}, the temperature at 10% CH_4 conversion,) of $LaMg_xMn_{1-x}Al_{11}O_{19}$ catalysts are close to 460 °C, which are lower than those of the catalysts at $x > 0.5$ (510–570 °C). It is well accepted that at low conversions, the combustion reaction was controlled predominately by the surface reaction [2]. The former catalysts contained higher Mn contents than the latter; therefore,

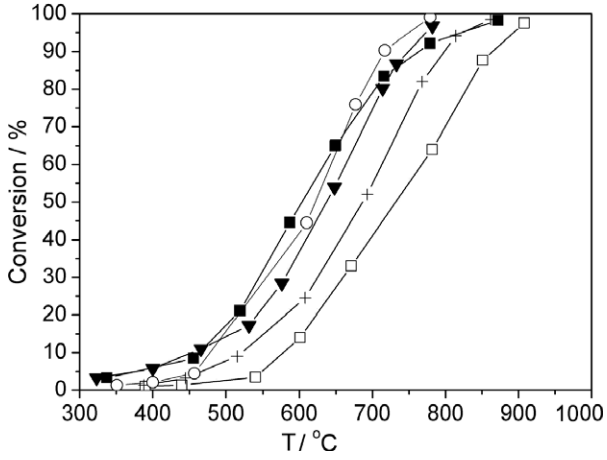

Fig. 8. Light-off curves of CH_4 combustion over $LaMg_xMn_{1-x}Al_{11}O_{19}$ catalysts, GSSV = 48 000 h^{-1}, 1 vol.% CH_4, 99 vol.% Air: (▼) $x = 0$; (■) $x = 0.2$; (○) $x = 0.5$; (+) $x = 0.8$; (□) $x = 1$.

the former exhibited high activity for CH_4 combustion. The complete combustion temperatures (T_{90}, the temperature at 90% CH_4 conversion,) of $LaMg_xMn_{1-x}Al_{11}O_{19}$ catalysts is in the range of 690–850 °C. At high conversions of CH_4, the combustion process usually includes surface reactions and free radical reactions [2]. The process is mainly predominated by free radical reactions, which are limited by the mass transfer process. The mass transfer limitation cannot be neglected; therefore, low surface area would limit the mass transfer of the reactants and T_{90} increased. As a result, $LaMg_{0.5}Mn_{0.5}Al_{11}O_{19}$ catalyst showed the highest activity ($T_{90} = 690$ °C) due to its highest surface area (40.1 $m^2\ g^{-1}$). It could be assumed that the simultaneous introduction of Mg and Mn significantly improved the activity and stability of MP catalyst through a synergetic effect of Mn and Mg. Mn promoted the formation of MP crystal; Mg stabilized the structure of MP crystal and made more Mn take on high oxidation state.

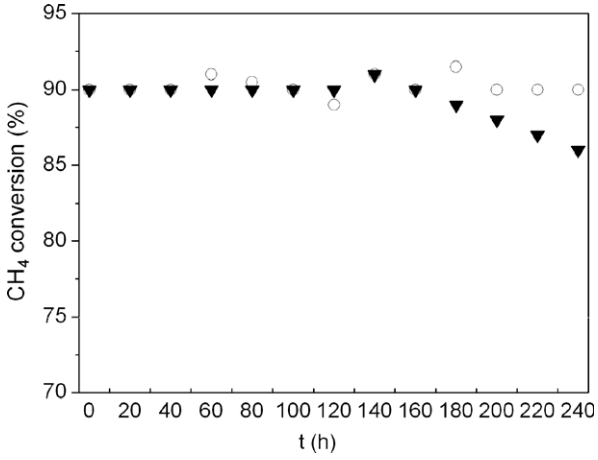

Fig. 9. Lifetime curves of $LaMg_{0.5}Mn_{0.5}Al_{11}O_{19}$ and $LaMnAl_{11}O_{19}$ catalysts. Test conditions: GSSV = 48 000 h^{-1}, 1 vol.% CH_4, 99 vol.% Air; 700 °C.

The variations of CH_4 conversion with reacting time under the reacting conditions was further investigated, while the reacting temperature was kept at 700 °C. Observed from Fig. 9, the CH_4 conversion over $LaMg_{0.5}Mn_{0.5}Al_{11}O_{19}$ catalyst did not decrease after reacting for 240 h; in contrast, the CH_4 conversion over $LaMnAl_{11}O_{19}$ catalyst decreased obviously after reacting for 160 h. After reaction of 240 h, the surface area of $LaMnAl_{11}O_{19}$ catalyst decreased from 29.7 to 22.5 $m^2 g^{-1}$; nevertheless, the surface area of the former did not nearly decrease (40.1 vs. 39.9 $m^2 g^{-1}$). This indicates that the doping of Mg and Mn favors to maintain thermal stability of the catalyst.

4. Conclusions

The activity and stability of MP catalyst was enhanced effectively through a synergetic effect of Mn and Mg. At a suitable atomic ratio of Mg to Mn, $LaMg_{0.5}Mn_{0.5}Al_{11}O_{19}$ had highest surface area (40.1 m g^{-1}) and activity ($T_{10} =$ 470 °C, $T_{90} = 690$ °C) for combustion of CH_4. Lifetime experiment showed that Mg introduction enhanced the stability of MP crystal.

Acknowledgement

This work is supported by Chinese National Science Foundation (Grants 20433010, 20571047), Chinese Postdoctoral Science Foundation (Grant 20060390057), and the Ministry of Science and Technology of P.R. China (G1999022401).

References

[1] L.D. Pfefferle, W.C. Pfefferle, Catal. Rev. Sci. Eng. 29 (1987) 219.
[2] M.F.M. Zwinkels, S.G. Jaras, P.B. Menon, T.A. Griffin, Catal. Rev. Sci. Eng. 35 (1993) 319.
[3] G. Groppi, C. Cristiani, P. Forzatti, Appl. B: Environ. 35 (2001) 137.
[4] M. Machida, K. Eguchi, H. Arai, J. Catal. 123 (1990) 477.
[5] B.W.L. Jang, R.M. Nelson, J.J. Spivey, M. Ocal, R. Oukaci, G. Marcelin, Catal. Today 47 (1999) 212.
[6] B.W. Jang, R.M. Nelson, J.J. Spivey, M. Ocal, R. Oukaci, G. Marcelin, Catal. Today 47 (1999) 103.
[7] R.C. Ropp, B. Carol, J. Am. Ceram. Soc. 63 (1980) 416.
[8] G. Groppi, M. Bellotto, C. Cristiani, P. Forzatti, P.L. Villa, Appl. Catal. A 104 (1993) 101.
[9] S. Matzuda, A. Kato, M. Mizumoto, H. Yamashita, Proceedings of the 8th ICC, vol. IV, Verlag, Basel, Berlin, 1984, p. 4.
[10] F. Teng, Z. Tian, Z. Wang, G. Xiong, Y. Xu, B. Wang, L. Wang, X. Yang, Z. Xu, In: Proceedings of the 13th International Congress on Catalysis (ICC13), Paris, France, 2004, p. 1.
[11] G. Groppi, M. Bellotto, C. Cristisni, P. Forzatti, P.L. Villa, J. Mater. Sci. 34 (1999) 2609.
[12] A.J. Zarur, J.Y. Ying, Nature 403 (2000) 65.
[13] D.L. Trimm, Appl. Catal. 7 (1983) 249.
[14] M. Machida, K. Eguchi, H. Arai, J. Catal. 103 (1987) 385.
[15] M. Gasperin, M.C. Saine, A. Kahn, F. Laville, M. Lejus, J. Solid State Chem. 54 (1984) 61.
[16] N. Iyi, Z. Inue, S. Takekawa, S. Kimura, J. Solid State Chem. 54 (1984) 70.
[17] D. Saber, A.M. Lejus, Mater. Res. Bull. 16 (1981) 1325.
[18] F. Teng, P. Xu, Z. Tian, G. Xiong, Y. Xu, Z. Xu, L. Lin, Green Chem. 7 (2005) 493.
[19] L. Lisi, G. Bagnasco, P. Ciambelli, S. De Rossi, P. Porta, G. Russo, M. Turco, J. Solid State Chem. 146 (1999) 176.
[20] E.R. Stobbe, B.A. De Boer, J.W. Geus, Catal. Today 47 (1999) 161.
[21] M. Bellotto, G. Artioli, C. Cristiani, P. Forzatti, G. Groppi, J. Catal. 179 (1998) 597.
[22] M. Machida, K. Eguchi, H. Arai, J. Catal. 120 (1989) 377.
[23] L. Laville, D. Gourier, A.M. Lejus, D. Vivien, J. Solid State Chem. 49 (1983) 180.
[24] J.-G. Park, A.N. Cormack, J. Solid State Chem. 130 (1997) 199.